Robinson, M. E., Nazemi, A., Lunn, D. J., Hayward, D. W., Boott, C. E., Hsiao, M. S., Harniman, R. L., Davis, S. A., Whittell, G. R., Richardson, R. M., De Cola, L., & Manners, I. (2017). Dimensional control and morphological transformations of supramolecular polymeric nanofibers based on cofacially-stacked planar amphiphilic platinum(II) complexes. *ACS Nano*, *11*(9), 9162-9175. https://doi.org/10.1021/acsnano.7b04069

Dimensional Control and Morphological Transformations of Supramolecular Polymeric Nanofibers Based on Cofacially-Stacked Planar Amphiphilic Platinum(II) Complexes

Matthew E. Robinson[†], Ali Nazemi[†], David J. Lunn[†], Dominic W. Hayward[†], Charlotte E. Boott[†], Ming-Siao Hsiao[§], Robert L. Harniman[†], Sean A. Davis[†], George R. Whittell[†], Robert M. Richardson[‡], Luisa De Cola[⊥], and Ian Manners*[,†]

[†] School of Chemistry, University of Bristol, Bristol, BS8 1TS, United Kingdom

[§]UES, Inc. and Materials & Manufacturing Directorate, Air Force Research Laboratory, Wright-Patterson AFB, Ohio 45433, United States

[‡] School of Physics, University of Bristol, BS8 1TS, United Kingdom

[⊥] ISIS & icFRC, Université de Strasbourg & CNRS, 8 Allée Gaspard Monge, 67000 Strasbourg, France

ABSTRACT: Square-planar platinum(II) complexes often stack cofacially to yield supramolecular fiber-like structures with interesting photophysical properties. However, control over fiber dimensions and the resulting colloidal stability is limited. We report the self-assembly of amphiphilic Pt(II) complexes with solubilizing ancillary ligands based on polyethylene glycol [PEG_n, where n = 16, 12, 7]. The complex with the longest solubilizing PEG ligand, **Pt-PEG$_{16}$**, self-assembled to form polydisperse one-dimensional (1D) nanofibers (diameters < 5 nm). Sonication led to short seeds which, on addition of further molecularly-dissolved **Pt-PEG$_{16}$** complex, underwent elongation in a "living supramolecular polymerization" process to yield relatively uniform fibers of length up to *ca*. 400 nm. The fiber lengths were dependent on the **Pt-PEG$_{16}$** complex to seed mass ratio in a manner analogous to a living covalent polymerization of molecular monomers. Moreover, the fiber lengths were unchanged in solution after 1 week and were therefore "static" with respect to interfiber exchange processes on this timescale. In contrast, similarly formed near-uniform fibers of **Pt-PEG$_{12}$** exhibited dynamic behavior that led to broadening of the length distribution within 48 h. After aging for 4 weeks in solution, **Pt-PEG$_{12}$** fibers partially evolved into 2D platelets. Furthermore, self-assembly of **Pt-PEG$_7$** yielded only transient fibers which rapidly evolved into 2D platelets. On addition of further fiber-forming Pt complex (**Pt-PEG$_{16}$**) the platelets formed assemblies *via* the growth of fibers selectively from their short edges. Our studies demonstrate that when interfiber dynamic exchange is suppressed, dimensional control and hierarchical structure formation is possible for supramolecular polymers through the use of kinetically-controlled seeded growth methods.

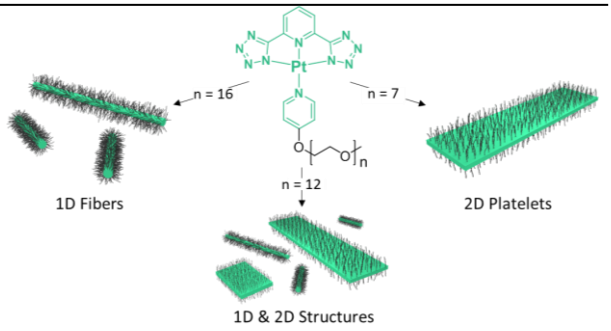

KEYWORDS: *self-assembly · kinetic control · metallophilic bonding · seeded growth · supramolecular structures*

The hierarchical self-assembly of molecular building blocks into functional one-dimensional (1D) supramolecular architectures through the exploitation of non-covalent interactions such as hydrogen bonding and π-π stacking has emerged as an important subfield of chemical science.[1-9] The tendency for supramolecular polymers to exhibit "dynamic" behavior where, unlike their covalent macromolecular counterparts, the building blocks can undergo exchange, gives rise to thermodynamically-controlled assembly and many desirable characteristics such as low viscosity processing and stimuli-responsive behavior.[3] Nevertheless, dynamic behavior poses a challenge in terms of the imposition of control over the dimensions, dispersities, and morphologies of the resulting structures, which is often desirable.[10-13]

Supramolecular polymers are commonly formed *via* a nucleation-elongation (cooperative growth) mechanism, in which an unfavorable nucleation step is followed by a favorable elongation cascade.[1,4,5] This process is analogous to the chain-growth covalent polymerization of molecular monomers in which initiation is followed by propagation. Suppression of the intrinsic dynamic exchange processes for supramolecular polymers is of interest as, in the absence of termination and transfer, this offers the intriguing possibility of accessing kinetically-controlled "living" supramolecular polymerizations analogous to the well-known living covalent polymerizations of organic monomers. The latter are of widespread importance as means of accessing polymers with chain length control, narrow length dispersities, and also complex architectures such as block and star copolymers.[1,11-18]

Crystallization is also a nucleation-elongation/growth process[19] and the solution self-assembly of block copolymers (BCPs) with a crystallizable core-forming block has received

considerable recent attention.[20-28] In selective solvents for the corona-forming block, these materials generally form 1D fiber-like micelles (for long corona segments) or two-dimensional (2D) platelets (for short corona segments) with crystalline cores.[20-28] These nanomaterials also appear to form *via* a crystallization-driven nucleation-elongation mechanism and are polydisperse in their length or areas, respectively, due to the slow nature of the initial, spontaneous nucleation step.[29] Sonication of fiber-like structures generates small seed micelles which permit seeded-growth on addition of further molecularly dissolved BCP (termed 'unimer').[30,31] Platelet micelles have also been shown to initiate growth where the addition of a fiber-forming unimer occurs at the short faces of the parent structure, producing 'tassels' of controlled length. Circumventing the slow nucleation step allows the formation of low dispersity 1D or 2D micelles with controlled dimensions *via* a process termed living crystallization-driven self-assembly (CDSA).[30-33] The sequential addition of different BCPs yields cylindrical or platelet block comicelles with segmented architectures.[30,34-37]

Square-planar transition metal-containing complexes based on Pt(II) or Au(III) have been of particular interest as precursors to supramolecular polymers.[38-48] These complexes have been shown to aggregate into discrete nanostructures by co-facial stacking of the planar species through metallophilic, π-π, and hydrogen-bonding interactions.[49,50] As a result of these non-covalent interactions, planar Pt(II) complexes have been reported to aggregate into a range of morphologies on the micron length scale, including fibers, ribbons and vesicles.[51-57] The resulting materials are of interest due to their electronic and emissive properties,[38] resistance to photobleaching,[58] low energy red or near IR excitation for bioimaging applications,[39] and potential anticancer activity.[42] Although alterations to the solvating ligands and solvent conditions can modify the aggregation behavior, most commonly thick, multi-micron long fibers are formed which rapidly result in gelation as a result of low colloidal stability. Control of the aggregation process is highly desirable as the ability to modulate fiber width and length should facilitate long-term colloidal stability, uniform behavior, and an ability to tune their optical and electronic properties.

Analogous seeded-growth techniques have been successfully applied to small molecule self-assembly under conditions of suppressed dynamic exchange. For example, Fukushima, Aida and coworkers and others have demonstrated the seeded growth of hexabenzocoronenes and the formation of supramolecular heterojunctions *via* the sequential addition of molecules with different electronic properties.[59-61] More recently, work on zinc(II) porphyrins,[62,64] perylene diimides,[61,65,66] and other self-assembling species[67] have shown that these small molecule building blocks form fibers that can then be converted into seeds and subsequently used to initiate seeded-growth polymerizations to form fibers of controlled length on the multi-micron length scale. Similarly, suppression of the dynamic nature of self-assembling protein and dithiol-functionalized peptidic building blocks has led to the formation of fibers, including segmented structures, using analogous approaches.[68,69]

Recently, we reported preliminary details on the successful seeded growth a of Pt(II) complex containing a solubilizing polyethylene glycol (PEG) ancillary ligand.[70,71]Herein, as a follow-up to our brief communication, we now report a detailed study of the hierarchical self-assembly of a series of square-planar Pt(II) complexes with varying chain lengths for the solubilizing oligomeric ancillary ligand and our attempts to impose dimensional control on the resulting one-dimensional assemblies.

RESULTS

Design and Synthesis of a Series of Amphiphilic Pt(II) Pincer Complexes For a systematic study of the self-assembly of square-planar Pt(II) complexes, three compounds were synthesized with varying lengths of the solubilizing PEG ancillary ligand. The square-planar complex that makes up the core-forming segment of the amphiphile was chosen due to its affinity for 1D growth, driven by Pt···Pt and π-π interactions.[72-74] Pairing this moiety with polymer chains of varying lengths at the ancillary ligand position was expected to produce assemblies with the Pt(II) complex at the core. The resulting morphologies were anticipated to be dependent on the degree of polymerization of the solvating PEG chain. The three pyridyl-functionalized solubilizing ligands were prepared from tosylated PEG_n monomethyl ether [where n represents the degree of polymerization (n = 16, number average molecular weight [M_n] = 890 g/mol; n = 12, M_n = 715 g/mol; n = 7, M_n = 495 g/mol; polydispersity index [PDI = M_w/M_n] of all three <1.1 as determined by matrix-assisted laser desorption ionization time-of-flight [MALDI-TOF] mass spectrometry)] and 4-hydroxy pyridine. A mixture of a solubilizing pyridyl-PEG_n ligand of desired molecular weight, $PtCl_2(DMSO)_2$, the N^N^N pincer ligand (di(1*H*-tetrazol-5-yl)pyridine) and *N*,*N*-diisopropylethylamine was refluxed in acetonitrile (MeCN) overnight (Scheme 1). After work-up, the purified materials were isolated as yellow solids in 66%, 71%, and 54% yield for PEG chain lengths of n = 16, 12, and 7 repeat units respectively. Characterization was achieved by ^{1}H and ^{13}C NMR spectroscopy, and MALDI-TOF mass spectrometry (for full characterization data see SI p. 4, 5 and Figures S1-15). For convenience, as the core-forming pincer ligand was a common feature, the complexes will be referred to as **Pt-PEG$_n$.**

Electronic Absorption and Fluorescence Spectra of Pt-PEG$_n$ Three separate chloroform solutions containing **Pt-PEG$_{16}$**, **Pt-PEG$_{12}$** and **Pt-PEG$_7$** at varying concentrations (0.7, 0.5, and 0.25 mg/mL respectively) were prepared and aged at 21 °C for 16 h. UV-Visible absorption spectra of the resulting solutions were collected at room temperature (Figure 1a). All spectra displayed the π-π* transition on the ancillary pyridine- and tridentate-ligand-centered (^{1}LC) charge transfers between 310 – 340 nm and the lower energy metal-to-ligand charge-transfer (^{1}MLCT) bands between 360 – 400 nm.[21] The characteristic metal-metal-to-ligand charge-transfer (^{1}MMLCT) observed in systems with metallophilic interactions between neighboring Pt atoms was detected at 430 nm (Figure 1a inset).[41,73-76] This transition arising from aggregates exhibited non-linear dependence of absorbance on concentration that thereby disobeys the Beer-Lambert law (Figure S16a).[74]

Scheme 1: Synthesis of **Pt-PEG$_n$** (where n = 7, 12, 16) [DIPEA = N,N – diisopropylethylamine]

All three **Pt-PEG$_n$** species exhibited a broad emission at 560 nm in chloroform (Figure 1b). The lack of a detectable difference in the emission spectra of the three compounds suggested

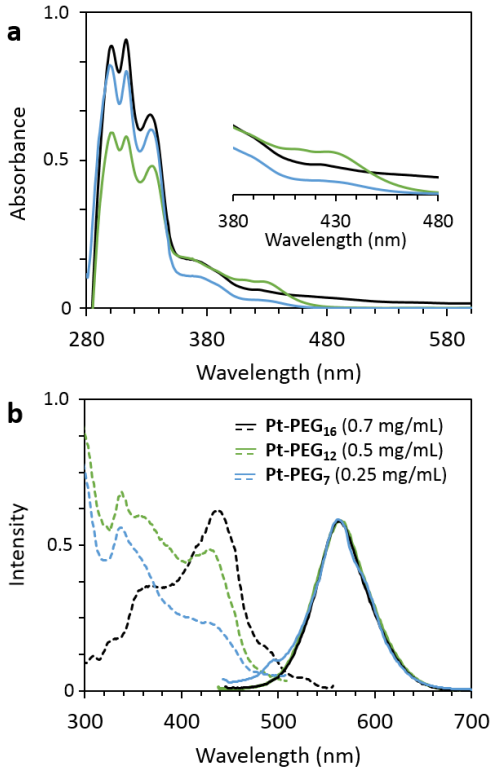

Figure 1: (a) UV-Vis absorption spectra of all three complexes in chloroform (Inset: enlarged region showing absorbance bands associated with the aggregate ^{1}MMLCT). (b) Excitation (dotted lines, λ_{em} = 560 nm) and emission (solid lines, λ_{ex} = 430 nm) spectra of **Pt-PEG$_n$** complexes in chloroform

that the Pt-Pt distance is not significantly affected by the solvation of longer or shorter ancillary ligand chains. The excitation spectra also reproduced the band found in the electronic absorption spectra at 430 nm (Figure 1b). These photophysical characteristics suggest that the aggregation of Pt(II) complexes produces ^{3}MMLCT states through communication between d_{z^2} orbitals on adjacent Pt(II) atoms.[41]

Self-Assembled Fibers from Pt-PEG$_{16}$

We first set out to study the nanofibers formed from the structure with the longest coronal chain, **Pt-PEG$_{16}$**. Previous studies of the **Pt-PEG$_4$** analogue have demonstrated the formation of long (> 100 μm) and relatively thick (>50 nm wide) fibers in organic solvents (*i.e.* dichloromethane and dimethylformamide) at room temperature that aggregate to form metallogels.[74] By employing a significantly longer solubilizing chain, we were able to produce thin, colloidally stable fibers that could be subsequently processed to control their lengths.

Length Control of Supramolecular Nanofibers Formed from Pt-PEG$_{16}$ by Seeded-Growth The general scheme for the preparation of fibers of controlled length is shown in Scheme 2. **Pt-PEG$_{16}$** was dissolved in chloroform at 0.05 – 5 mg/mL and aging the samples overnight at 21 °C produced clear yellow solutions. Fibers were imaged in their dried state

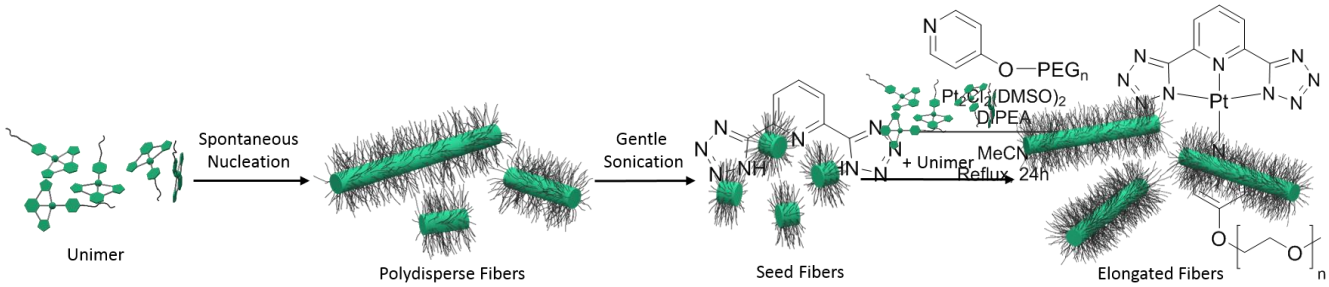

Scheme 2: Schematic representation of the formation of fibers from **Pt-PEG$_{16}$**, their sonication into seed fibers and the subsequent unimer addition that leads to fibers of controlled length

by transmission electron microscopy (TEM) and in solution by confocal laser scanning microscopy (CLSM) which revealed the formation of polydisperse 1D structures (*e.g*. in chloroform - L_n = 206 nm, L_w/L_n = 1.73, σ/L_n = 0.85 where L_n and L_w are the number and weight average length, and σ is the standard deviation, Figure 2a,b, S16b). Fibers formed by analogous Pt(II) complexes with shorter, less bulky solubilizing ligands have been reported to possess diameters greater than 100 nm.[71,73-75] The fibers formed by **Pt-PEG$_{16}$**, however, are substantially smaller in diameter (< 5 nm) (Figure 2a inset) and do not aggregate into large networked bundles. Even when aged at 21 °C for over 6 months, the fibers retained their small diameters and colloidal stability (Figure S17). Fibers were also formed when **Pt-PEG$_{16}$** was dissolved in a number of other solvents. For example, 0.5 mg/mL solutions of **Pt-PEG$_{16}$** that had been aged for 16 h at 21 °C in MeCN or dimethylformamide (DMF) (Figure 2c and d respectively) produced fibers with lengths greater than 600 nm and the same narrow diameter. When the MeCN solution was drop-cast, evaporated to dryness, and analyzed by TEM, the resulting micrographs displayed a large amount of unimer-derived film, indicative of incomplete aggregation. The solution in MeCN also exhibited a decrease in the absorption due to stacking at 430 nm when heated to elevated temperatures (Figure S19). We observed no fibers when an aliquot of the MeCN solution at 80 °C was drop-cast and analyzed by TEM (Figure S19a). This indicated the return of fibers to their molecularly dissolved unimer state is triggered at elevated temperatures.

Ultrasonication of BCP cylinders is an established method for forming short seed micelles.[32] First, sonicating a 0.1 mg/mL chloroform solution of polydisperse **Pt-PEG$_{16}$** fibers at 0 °C for 1 h produced seed fibers (L_n = 54 nm, L_w/L_n = 1.11 σ/L_n = 0.33) which were characterized by atomic force microscopy (AFM) (Figure 3a) and TEM (Figures S21a, S22a). We then applied the seeded-growth approach developed for the living CDSA of BCPs. Fiber length was controlled through additions of varying amounts of **Pt-PEG$_{16}$** in their unimeric state to the seed fibers. Consequently, 10, 20, 30, 40, 50, 60. 80, and 160 μg of unimeric **Pt-PEG$_{16}$** were added as a 2 mg/mL solution in hot (80 °C) MeCN to 20 μg of seeds in chloroform at 21°C. The resulting solutions were aged for 16 h at 21 °C, then drop-cast and analyzed by AFM (Figure 3b - g) and TEM (Figures S21 and S22). Statistical analysis confirmed that the L_n of the resulting fibers was linearly dependent on the unimer-to-seed mass ratio (Figure 3h) and that fibers up to L_n = 354 nm (Figure 3g) could be produced with relatively low length distributions (L_w/L_n < 1.25 based on TEM data, see SI Figures S21, S22 and Table S1 for full seeded-growth data). It is also notable that the micrographs display a distinct lack of seed fibers after the addition of unimer. This is indicative of the seeds being consumed during the controlled growth. A control experiment was also performed in which 20 μg of unimeric **Pt-PEG$_{16}$** in hot (80°C) MeCN was added to a similar volume of chloroform in the absence of seeds. TEM micrographs of the resulting samples displayed the formation of polydisperse fibers (L_n = 164 nm, L_w/L_n = 1.99, Figure S25). The seeded growth experiment in which the same 20 μg of **Pt-PEG$_{16}$** unimer was instead added to 20 μg of seed fibers produced fibers with a narrow length distribution (L_n = 54 nm, L_w/L_n = 1.22). Comparing these length distributions for homogeneous nucleation with those for seeded growth (Figures S25a and S24c respectively) demonstrated that the formation of low dispersity fibers could occur only in the presence of seed initiators.

The fibers formed by many other self-assembling small-molecule systems have been reported to be dynamic with respect to the exchange of their unimer building blocks.[1-10] To determine if our system would exhibit analogous dynamic behavior, and therefore compromise the dimensional stability of the **Pt-PEG$_{16}$** fibers, we monitored the L_n and length distribution (L_w/L_n) of a solution of short fibers (L_n = 65 nm, L_w/L_n = 1.17, Figure S26a, S27a) during the course of a 1 week period. The fibers that were dried and then analyzed by electron microscopy in this time frame were, within experimental error, unchanged with respect to L_n and L_w/L_n (Figure S26, S27, Table S3). In a similar experiment, we examined the same parameters for a **Pt-PEG$_{16}$** seed solution (L_n = 54 nm, L_w/L_n = 1.11) aged at 21 °C for 3 months. The resulting seed fibers had doubled in length and increased in dispersity (L_n = 103 nm, L_w/L_n = 1.34, Figure S28). These results suggest that a slow dynamic exchange between the seed fibers occurs during extensive aging in solution. However, clearly over the timescale of the seeded-growth experiments (*i.e.* 48 h), the dynamic exchange is sufficiently suppressed to permit length control and relatively low dispersity length distributions.

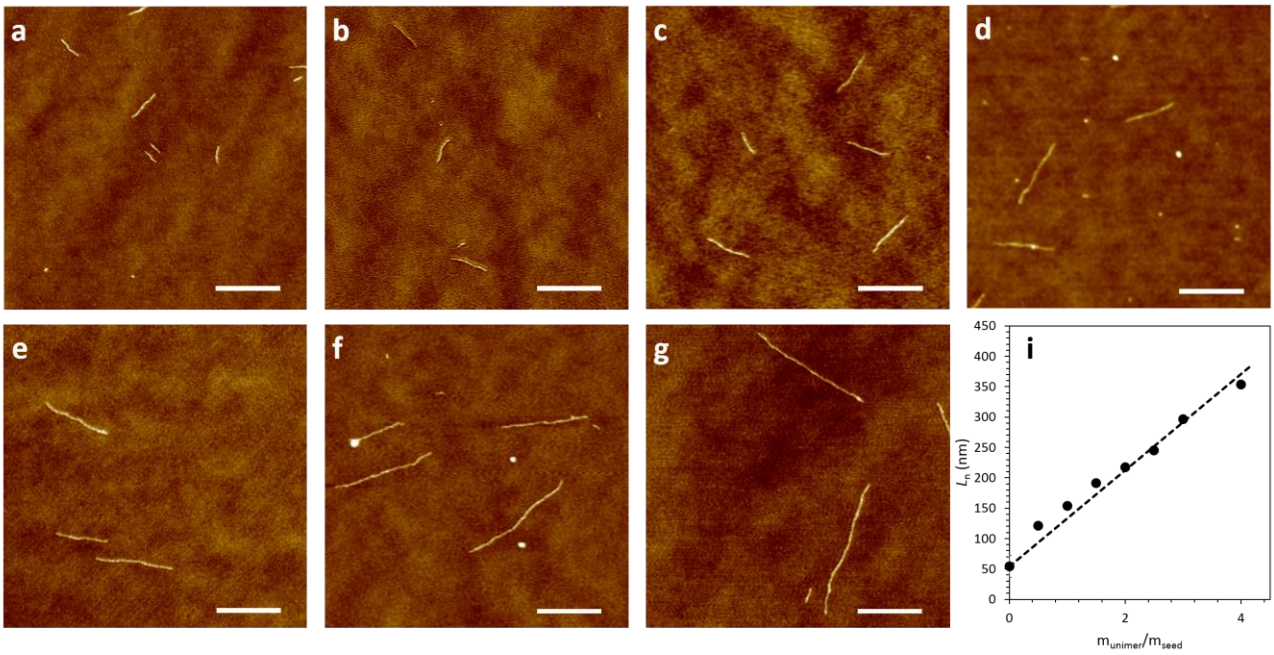

Figure 3: Representative AFM micrographs of (a) 0.5 mg/mL chloroform solution of **Pt-PEG$_{16}$** seed fibers after sonication (L_n = 41 nm, L_w/L_n = 1.06). Elongated fibers formed by adding (b) 10 μg, (c) 20 μg, (d) 40 μg, (e) 50 μg, (f) 60 μg, and (g) 80 μg of **Pt-PEG$_{16}$** unimer to 20 μg of seed fibers in chloroform. (h) Linear dependence of the fiber average contour length on the unimer-to-seed mass ratio. Scale bars: 250 nm.

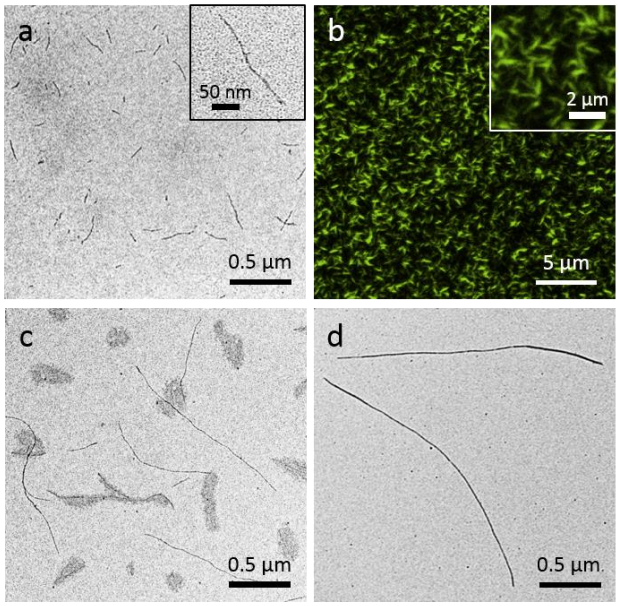

Figure 2: Fibers formed by aging a 0.25 mg/mL chloroform solution of **Pt-PEG$_{16}$** at 21 °C for 16 h imaged by (a) TEM (inset higher magnification of single fiber) and (b) CLSM (inset: higher magnification of fluorescent fibers). Representative TEM micrographs of polydisperse fibers formed by aging a 0.5 mg/mL solution for 16 h at 21 °C in (c) MeCN and (d) DMF.

Solid- and Solution-State Structural Characterization of Pt-PEG$_{16}$ Fibers Previous studies on Pt(II) complex self-assembly have enabled a determination of the inter-complex spacing mediated by the Pt···Pt and π-π overlap through single-crystal X-ray diffraction. Perhaps due to the nature of the ancillary PEG ligand, which consisted of a distribution of oligomeric chain lengths, the purified complex was a gum that was unsuitable for the growth of single crystals. We therefore applied other characterization techniques on both the dried and solvated fibers to discern the nature of the complex packing within the structures' core.

In order to complement the TEM characterization, which is performed in the dried state, and the CLSM data in solution

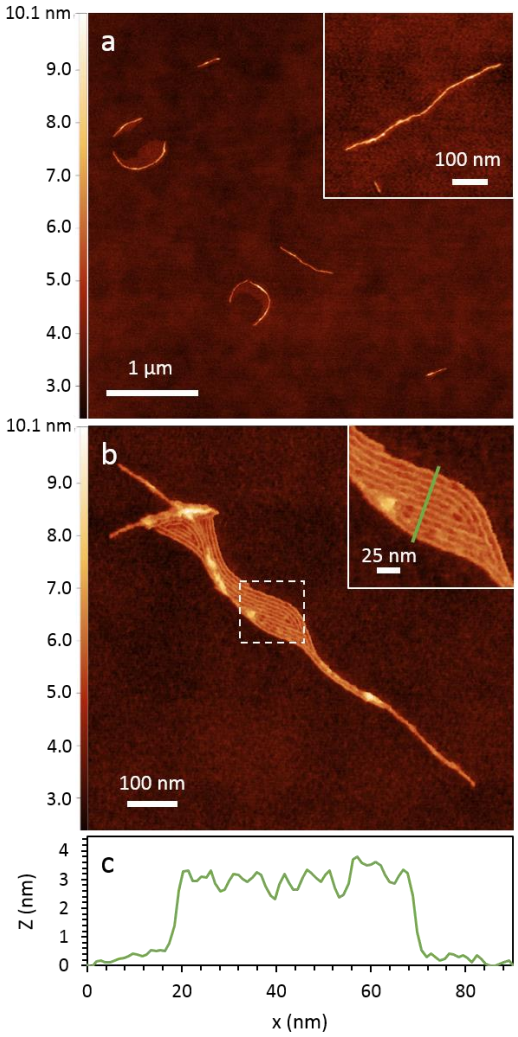

(Figure 2b), we also examined the fibers in the solution-phase by small-angle X-ray scattering (SAXS). Initial attempts to characterize the fibers in chloroform were unsuccessful due to X-ray absorption and we therefore explored the use of DMF as solvent. **Pt-PEG$_{16}$** was dissolved in DMF to make a 5 mg/mL solution. After aging the mixture for 16 h at 21 °C, an aliquot was drop-cast onto a copper grid and analysis by TEM revealed a high surface density of fibers (Figure S29a). Another aliquot of the same solution was then sealed in a capillary tube and was analyzed by SAXS. The resulting SAXS trace of the radially-averaged and background subtracted scattering (Figure S29b) showed that the intensity at low scattering vector exhibited a $Q^{-0.96}$ dependence, indicating the presence of elongated or rod-like structures in solution.[24] The data collected represented an intermediate Q-region, as indicated by the gradient persisting at the lowest Q-values suggesting that the fibers in solution are very long. Assuming the fibers have a circular cross-section and following the intermediate-Q Guinier approximation, the data suggest a core radius of 1.6 nm (and therefore width of 3.2 nm) for the **Pt-PEG$_{16}$** fibers in solution (Figure S29c).

In addition, a 0.5 mg/mL chloroform solution of **Pt-PEG$_{16}$** fibers was drop-cast and imaged by AFM (Figure 4). The resulting micrographs displayed fibers with narrow diameters (<5 nm) comparable to the widths determined by TEM. Fiber lengths also ranged in length from 300 nm to several microns

(Figure 4a,b). A height analysis (Figure 4c) across multiple fibers showed the structures to be about 3.3 nm high – in good agreement with core width determined by SAXS.

Further structural characterization of the fibers by wide-angle X-ray scattering (WAXS) and selected area electron diffraction (SAED) was performed. An aliquot of the 5 mg/mL DMF solution containing **Pt-PEG$_{16}$** fibers was also drop-cast and evaporated on a Kapton® film and the residual fibers subjected to WAXS analysis. The resulting plot (Figure S29d) displayed a strong Bragg peak (Q = 1.891 Å^{-1}, d = 0.330 nm) assigned to the distance between cofacially stacked Pt complexes at the fiber core. In addition, SAED of the fibers (Figure S29e,f) also showed a distinct reflection with a spacing of 0.323 nm, a value that is within the known range of spacings for stacked Pt complexes that exhibit metallophilic interactions.[48,77]

Next, we explored the effect of fiber length on the UV-vis absorption spectra of **Pt-PEG$_{16}$**. We targeted very short fibers to provide a lower limit for our comparative data. Previous reports of seed formation through high-powered ultrasonication of BCP cylinders with a sonotrode device suggest that increasing the sonotrode unit power will easily yield much shorter seed micelles.[31,78] The resulting micrographs produced by drop-casting an ultrasonicated 0.25 mg/mL chloroform solution of **Pt-PEG$_{16}$** displayed no evidence of surviving seed fibers. Fiber cleavage in a sonication bath at 0 °C, however, was found to be more controlled, and these milder conditions were therefore used over 3 h to produce short seed fibers (L_n = 32 nm (L_w/L_n=1.10, Figure S30). Interestingly, the shortest fibers showed no major difference in their UV-vis absorption spectra when compared to the longer structures (Figure S30g). The lack of any detectable shift in these spectra suggests that the maximum conjugation limit is even shorter than the minimum fiber length (*ca.* 30 nm) available in this study.

Self-Assembly of Pt-PEG$_{12}$

Following the studies of the self-assembly of **Pt-PEG$_{16}$,** we moved on to explore the aggregation behavior of **Pt-PEG$_{12}$**, a complex with a shorter ancillary solubilizing ligand.

Figure 4: (a,b) AFM height images of representative **Pt-PEG$_{16}$** fibers grown in chloroform at 0.5 mg/mL (Inset: higher magnification of multiple parallel fibers) and (c) height profile of multiple fibers (green line trace in b).

Pt-PEG$_{12}$ was dissolved in chloroform at 0.5 mg/mL and allowed to age 16 h at 21 °C. This solution was drop-cast and the subsequent TEM analysis revealed that fibers formed were similar in length (> 200 nm) and width (< 5 nm) to their **Pt-PEG$_{16}$** counterparts (Figure 5a). There was no detectable unimer film present on the copper grid and the average length (L_n) of the **Pt-PEG$_{12}$** fibers was 453 nm (L_w/L_n = 1.63, σ/L_n = 0.80, Figure S31a,b). These fibers were then sonicated and used in a seeded growth process identical to their **Pt-PEG$_{16}$** contemporaries. First, a 0.1 mg/mL chloroform solution of polydisperse length **Pt-PEG$_{12}$** fibers was sonicated at 0 °C for 1 h to produce seed fibers (L_n = 38 nm, L_w/L_n = 1.11, Figure 32a, S33a). The resulting fiber contour length was then controlled through the additions of **Pt-PEG$_{12}$** unimer to these seeds. 10, 20, and 40 μg of unimeric **Pt-PEG$_{12}$** was added from an 80 °C MeCN solution to 20 μg of seed fibers in chloroform. The solutions were then aged for 16 h at 21 °C and then an aliquot was drop-cast and imaged by TEM. Analogous to the seeded growths of **Pt-PEG$_{16}$**, the resulting fiber lengths increased linearly with the unimer-to-seed mass ratio (Figure S32, S33 and Table S4). The resulting fibers after the largest unimer addition (40 μg, m_{unimer}/m_{seed} = 2) reached L_n = 438 nm (L_w/L_n = 1.28).

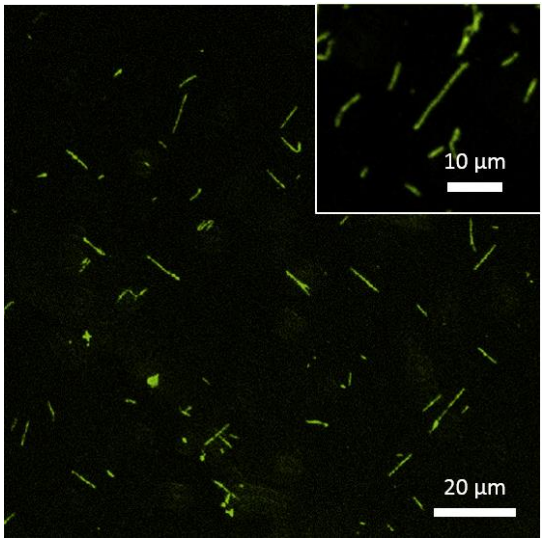

Figure 6: CLSM image of fibers and platelets formed from **Pt-PEG$_{12}$** in chloroform.

We also tested the potential for **Pt-PEG$_{12}$** to exhibit dynamic exchange behavior by monitoring the L_n and polydispersity (L_w/L_n) of near monodisperse length fibers over the course of 1 week. A solution of short **Pt-PEG$_{12}$** fibers (L_n = 61 nm, L_w/L_n = 1.08, Figure S34a, S35a) in chloroform was aged at 21 °C and was drop-cast onto a copper grid at 24 h intervals. Length analysis of the resulting TEM micrographs revealed the increase in both L_n and L_w/L_n in as little as 48 h (Figure S34, S35 and Table S5). After 120 h in solution, the L_n had tripled to 183 nm and the polydispersity had significantly increased (L_w/L_n = 1.40). When compared to the analogous study with **Pt-PEG$_{16}$**, **Pt-PEG$_{12}$** is notably more dynamic with respect to inter-fiber building-block exchange.

Interestingly, the fibers formed by **Pt-PEG$_{12}$** in chloroform evolved into platelet structures after aging the solution for extended periods of time (*ca*. 4 weeks). After 4 weeks in solution at 21 °C, a drop-cast aliquot was analyzed by TEM to reveal a distinct new platelet morphology alongside polydisperse length fibers (Figure 5b, S31c). Through the analysis of higher magnification electron micrographs, the majority of the platelets displayed a distinct boundary where 1D fibers protruded from the 2D structures (Figure 5c, S31d). The coexistence of both platelet and fiber morphologies still persisted after 6 months of aging in solution (Figure S36). The platelets of **Pt-PEG$_{12}$** require 4 weeks to form but are sufficiently robust to allow solvent removal and redispersion without major fracturing or disassembly (Figure S36b).

Figure 5: TEM micrographs of **Pt-PEG$_{12}$** nanostructures drop cast from a 0.5 mg/mL chloroform solution after being aged at 21 °C for (a) 16 h and (b) 4 weeks. (c) A higher magnification of a platelet terminus. (d) A schematic demonstrating the transformation of the unimer into platelets *via* fiber intermediates. (e) AFM height image of a 0.5 mg/mL chloroform solution drop cast onto a carbon coated copper grid and (f) height profile of a platelet and fiber (green line in e).

AFM analysis of the mixture of self-assembled fibers and platelets formed by **Pt-PEG$_{12}$** was also performed (Figure 5e, S31e). A height trace measurement of both morphologies confirmed that the platelets were flat and were of similar height to the fibers (~3.2 nm) (Figure 5f).

Solution- and Solid-State Characterization of Pt-PEG$_{12}$ Platelet Structures Compared to their fiber counterparts, the platelets formed by **Pt-PEG$_{12}$** possess dimensions significantly longer (>5 µm) and wider (~20 - 30 nm) allowing them to be readily detected by CLSM (Figure 6, S31f). Despite their relatively large size, the platelets demonstrate impressive colloidal stability and remain dispersed in solution for over 6 months, along with the co-existing fibers. To further characterize the 2D platelets X-ray scattering techniques were employed. First, a 5 mg/mL DMF solution of **Pt-PEG$_{12}$** containing platelets and fibers was prepared. A 20 µL aliquot of this solution was then drop-cast onto a Kapton® film, dried and then subjected to WAXS analysis (Figure S31g). The intense scattering at 1.902 Å^{-1} - also detected in the **Pt-PEG$_{16}$** fiber solutions - can be attributed to the 0.330 nm spacing between the cofacially stacked Pt complexes. In addition, SAED of a single **Pt-PEG$_{12}$** platelet (Figure S31h,i) also showed a distinct reflection with a spacing of 0.323 nm, analogous to the value detected for **Pt-PEG$_{16}$**. This consistent inter-complex distance is mirrored clearly in the MMLCT transitions detected by electronic absorption (430 nm) and emission (broad peak centered at 560 nm) when comparing the assemblies formed by **Pt-PEG$_{12}$** and **Pt-PEG$_{16}$**.

Scarf-like Nanostructures of Pt-PEG$_{12}$ Platelets and Pt-PEG$_{16}$ Fibers Next, we aimed to reduce the overall size and aspect ratio of the **Pt-PEG$_{12}$** platelets formed during the extended solution aging process. By subjecting a chloroform solution containing mixed platelet and fiber morphologies (Figure 7b) to gentle sonication (30 minutes at 0 °C), we were able to fragment both into much smaller components (Figure 7c, S37). The platelets present after sonication also exhibited square-edges without any fiber tendrils, adopting a more rectangular shape compared to their precursors. We then attempted to produce a mixed fiber-platelet hybrid structure by initiating the growth of the fiber-forming, longer PEG chain material (**Pt-PEG$_{16}$**) from the shorter PEG chain-containing platelets (**Pt-PEG$_{12}$**) (Figure 7a). To a 0.1 mg/mL chloroform solution at 21 °C containing sonicated **Pt-PEG$_{12}$** platelets and fibers was added 30 µg of **Pt-PEG$_{16}$** unimer in MeCN at 80 °C. The solution was aged at 21°C for 16 h and then an aliquot was drop-cast onto a TEM grid. TEM analysis confirmed the growth of **Pt-PEG$_{16}$** fibers from the narrow faces of approximately 70% of the **Pt-PEG$_{12}$** platelets (Figure 7d, S38). The

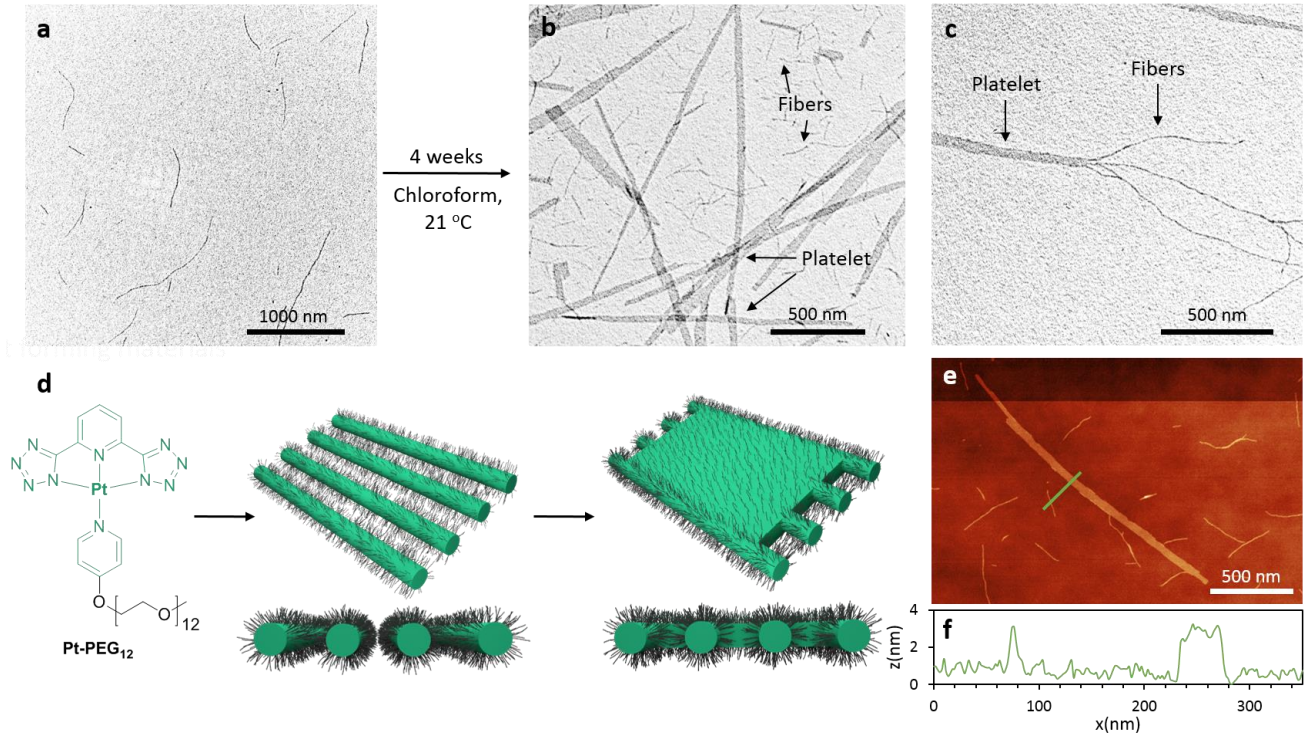

TEM micrographs also do not display any surviving short seed fibers, instead, a number of long fibers are present. Thus, the addition of **Pt-PEG$_{16}$** to the fragmented **Pt-PEG$_{12}$** fibers and platelets leads to the new scarf-like structures as well as elongated fibers *via* seeded growth.

Self-Assembly of Pt-PEG$_7$

The aforementioned results showed that reducing the ancillary PEG ligand chain length from 16 to 12 repeat units leads to an increase in dynamic behavior and triggers a morphological transition from fibers to a mixture of fibers and platelets. Next, we explored the use of a PEG ligand chain length of only 7 repeat units. When a 0.5 mg/mL chloroform solution of **Pt-PEG$_7$** was aged at 21 °C for 24 h, a drop-cast aliquot showed the exclusive presence of 2D platelets by TEM (Figure 8a, S39). The resulting multi-micron long ribbons possessed their greatest widths (~ 60 nm) at the center of the structure and tapered off towards the termini. Once formed, the ribbon-like platelets could also be dried and redispersed in chloroform without incurring any detectable change in overall dimensions (Figure S40). The 24 h period during which **Pt-PEG$_7$** formed the platelet morphology allowed us to monitor the transformation from unimer by TEM by drop-casting the solution at specific time points (Figure 8b–e, S41). Immediately after dissolution, TEM analysis revealed what appeared to be short fibers (< 5 nm diameter) embedded in a unimer film (Figure 8b) that presumably forms as the result of a drying effect. After aging for 1 h at 21 °C, long fibers started to emerge (Figure 8c) and further aging to 16 h showed that only very long (> 3 μm) fibers remained (Figure 8d). In contrast, after 24 h, only platelet structures were detected (Figure 8e).

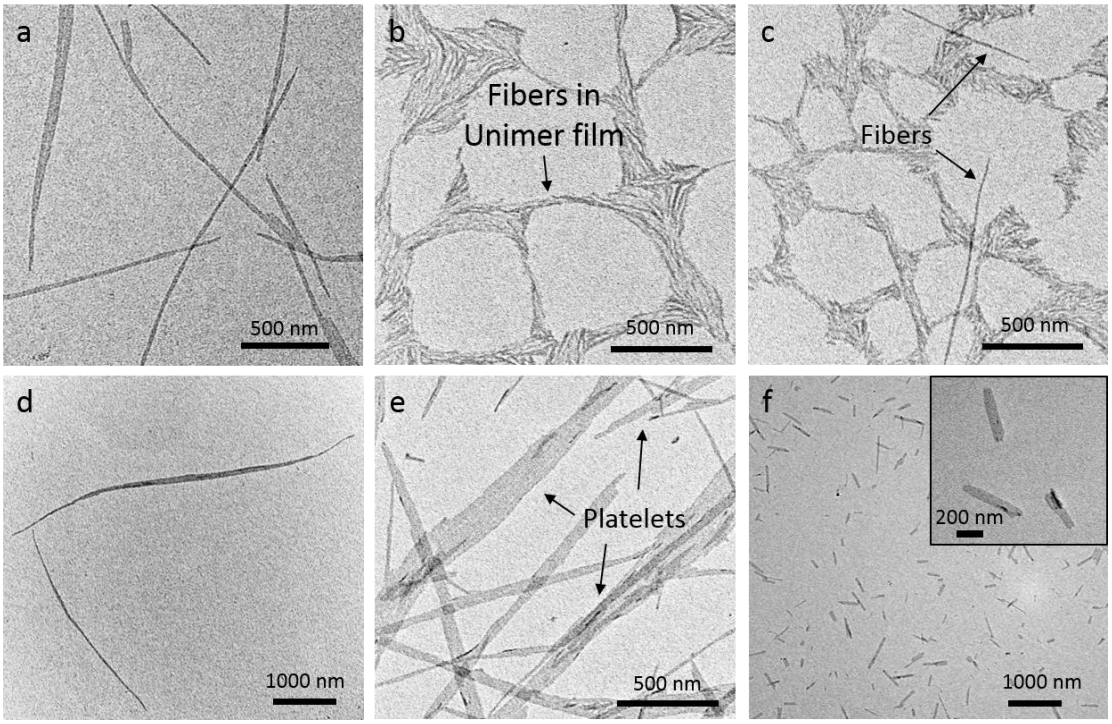

Figure 8: Platelets formed from **Pt-PEG$_7$** at 0.5 mg/mL in chloroform after aging for 24 h. Platelet growth monitored by dissolving **Pt-PEG$_7$** at 0.5 mg/mL in chloroform and drop-casting onto TEM grids at t = (b) 0 h, (c) 1h, (d) 16 h and (e) 24 h. (f) The resulting structures after 0.5 h of sonication at 0 °C (Inset: magnified small aspect ratio platelets).

To explore the possibility of producing platelet-type seed micelles, these 2D structures were then subjected to 30 minutes of sonication at 0 °C. This resulted in the formation of rectangular platelets with smaller aspect ratios (A_n = 11480 nm^2, A_w/A_n = 1.58, σ/A_n = 0.73, where A_n and A_w are the number and weight average surface areas, Figure 8f, S42). Similar to the **Pt-PEG$_{12}$** platelets, the 2D structures produced by **Pt-PEG$_7$** could also be used to initiate the growth of **Pt-PEG$_{16}$** fibers. To 200 µL of a 0.1 mg/mL chloroform solution of **Pt-PEG$_7$** at 21 °C was added 30 µg of **Pt-PEG$_{16}$** unimer in MeCN at 80 °C. The resulting solution was aged for 16 h at 21 °C, followed by drop-casting and analysis by TEM. The resulting electron micrographs revealed the growth of single fibers from the short faces of *ca.* 70% of the seed platelets (Figure S43). The original square-edged platelets also appeared to become more lenticular and also fiber-like towards their termini. The

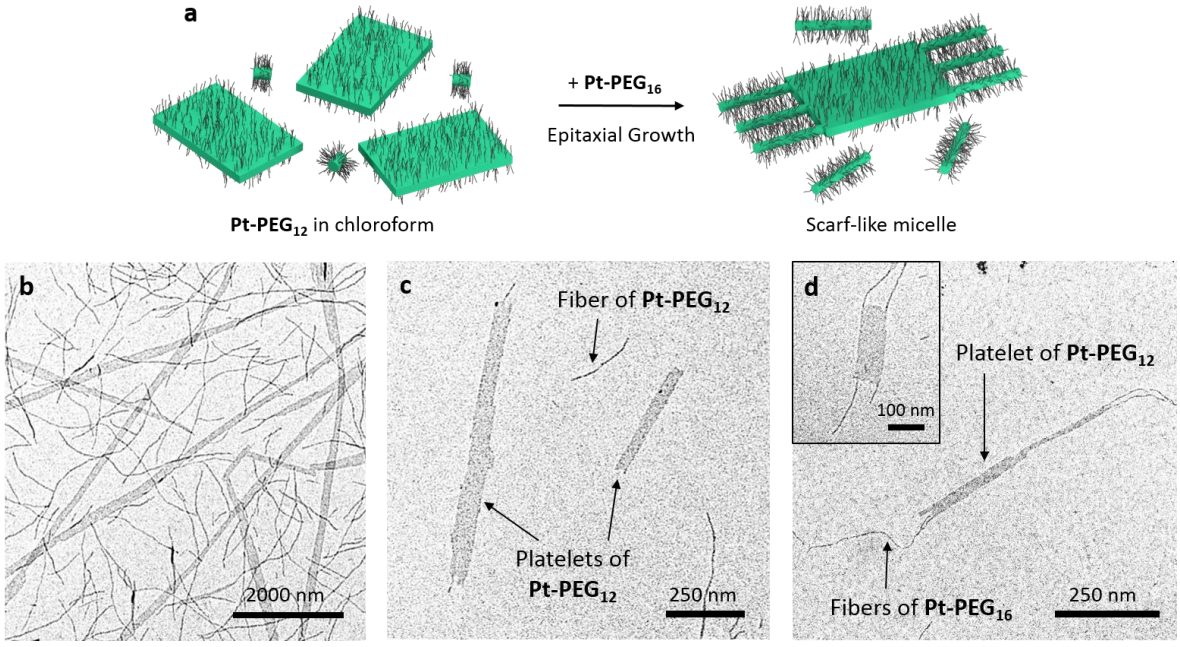

Figure 7: (a) A schematic demonstrating the addition of **Pt-PEG$_{16}$** selectively to the short faces of a **Pt-PEG$_{12}$** platelet. A drop cast aliquot of a 0.5 mg/mL chloroform solution containing polydisperse fibers and platelets of **Pt-PEG$_{12}$** (b) before and (c) after gentle sonication at 0 °C for 0.5 h. (d) Scarf-like hybrid structures formed by adding **Pt-PEG$_{16}$** to **Pt-PEG$_{12}$** platelets (Inset: a scarf structure grown from a significantly smaller platelet initiator).

addition of **Pt-PEG$_{16}$** also led to the formation of self-nucleated fibers alongside the platelet-fiber hybrid structures.

To gain insight into the nature of the stacking in the cores of the **Pt-PEG$_7$** platelets, we prepared a 5 mg/mL solution in DMF. An aliquot was drop-cast and, after the solvent evaporated, subject to TEM analysis. Simultaneously, a second aliquot was drop-cast onto a Kapton® film and analyzed in the dry state by WAXS. The TEM micrograph indicated the presence of a high surface density of platelets (Figure S44a). WAXS analysis led to the detection of a similar scattering peak to that observed for **Pt-PEG$_{12}$** and **Pt-PEG$_{16}$** (d = 0.330 nm, Figure S44b). Thus this peak can be similarly assigned to the spacing between the cofacially stacked square planar Pt moieties in the fiber core. SAED was also performed on **Pt-PEG$_7$** platelets (Figure S44c,d) and again a 0.323 nm reflection was detected and assigned to the inter-complex stacking distance. The similarity of this spacing in the fibers formed by all three Pt complexes is also evidenced by the near-identical electronic absorption and emission spectra (Figure 1). This demonstrates that this transition, which arises due to Pt···Pt interactions, is independent of the length of the solubilizing PEG ligand within the error of our measurements.

DISCUSSION

Length Control of 1D Nanostructures from Pt-PEG$_{16}$ and Pt-PEG$_{12}$ We have successfully applied the seeded growth "living CDSA" methods developed for BCP systems with crystallizable cores to self-assemble amphiphilic Pt(II) complexes with long solubilizing ancillary PEG ligands. A 16-repeat unit PEG-containing Pt(II) complex **Pt-PEG$_{16}$** was found to self-assemble exclusively into narrow diameter, colloidally stable nanofibers with controllable lengths and relatively narrow length distributions *via* a seeded-growth procedure. A key requirement for these metallosupramolecular fibers to be formed with length control and low dispersities is that dynamic exchange of the individual Pt(II) complex building blocks is suppressed on the time scale of the experiments (< 48 h). This was found to be the case for **Pt-PEG$_{16}$** and, to a lesser extent, **Pt-PEG$_{12}$**.

Previous work on similar Pt(II) complexes but without the long solubilizing ancillary PEG ligands has often demonstrated the formation of gels through uncontrolled spontaneous nucleation and large diameter (> 100 nm), multi-micron long fibers.[72-74,79-81] Length control has been recently established in one recent case[71] which uses a Pt(II) complex similar to those used in this study except that the PEG ligand possessed only 3 repeat units. Using much larger seeds (hydrodynamic diameter [D_h] = 265 nm as determined by dynamic light scattering) uniform fiber-like rods were grown to multi-micron lengths and hundreds of nanometers thick.[71] The fibers formed by **Pt-PEG$_{16}$** in this study however, are orders of magnitude narrower in diameter and are stable in solution (*i.e.* without gelling or uncontrolled aggregation) for long periods of time (> 6 months). Furthermore, the fibers formed *via* seeded growth have tunable lengths with relatively narrow length distributions up to *ca.* 400 nm dependent on the unimer-to-seed mass ratio.

In a seeded growth using **Pt-PEG$_{16}$** seeds (L_n = 60 nm, L_w/L_n = 1.14, Figure S23, S24), the contour lengths predicted by the unimer-to-seed mass ratios are smaller than those observed. This is particularly noticeable in the difference between the L_n of the seeds (60 nm) and the fibers after the addition of 5 µg (m_{unimer}/m_{seed} = 0.25) of unimer (observed L_n = 150 nm, expected L_n = 75 nm). This discrepancy has been noted in previous stud-

ies of crystalline-coil BCPs[82] and may be the result of two phenomena. First, the seeds may be thicker than the fibers that grow from their termini and second, a number of the initial seed structures could be inactive towards epitaxial growth.[82] Another issue arising from the studies was the significant dispersity increase for fibers above unimer-to-seed mass ratios of 4:1. At these higher ratios which correspond to larger unimer additions, the competition between epitaxial growth from the seeds and self-nucleation is most likely significant. This could result in the formation of new fibers *via* homogeneous nucleation in parallel to those undergoing elongation by seeded growth.

The suppression of dynamic unimer exchange for **Pt-PEG$_{16}$** fibers was demonstrated by monitoring the average fiber length and polydispersity over the course of 1 week. Over this time frame, neither a change in length nor distribution broadening was detected. Analogous experiments with **Pt-PEG$_{12}$** fibers revealed a significant increase in length and polydispersity in just 48 h. Furthermore, aging solutions of **Pt-PEG$_{12}$** for 4 weeks resulted in the additional formation of a 2D (*i.e.* platelet) morphology. The increase in dynamic behavior exhibited by **Pt-PEG$_{12}$** compared to **Pt-PEG$_{16}$** underscores the necessity for a long solubilizing ligand in order to suppress dynamic exchange.

Accessing 2D and Hierarchical Structures from Pt-PEG$_{12}$ and Pt-PEG$_7$ The main factor influencing the aggregation behavior of the **Pt-PEG$_n$** system studied in this work was found to be the degree of polymerization (n) of the solubilizing ancillary ligand. By reducing the length of the solubilizing PEG ligand, we have been able to access 2D structures. Thus, solutions of **Pt-PEG$_{12}$** initially produced 1D fibers comparable to those observed exclusively for the longer chain analogue **Pt-PEG$_{16}$** whereas multi-micron long platelets were also formed after aging in solution for 4 weeks. Interestingly, chloroform solutions containing **Pt-PEG$_7$** produced exclusively platelet morphologies over a significantly shorter time frame (*ca*. 24 h). The fact that the **Pt-PEG$_{12}$** solutions contained both platelets and fibers potentially suggests this PEG chain length characterizes a boundary between the two morphologies. Due to the nature of polymer synthesis, there are distributions of chain lengths present in the **Pt-PEG$_{12}$** material centered at n = 12. It is possible that the chains where $n \geq 12$ are the structures that remain as fibers even after 6 months, whereas platelets are slowly formed when $n < 12$.

Previous work from the Yam group on the self-assembly of amphiphilic planar Pt(II) complexes (Figure 9) revealed a morphological transition from fibers to platelets when the length of the core-forming alkyl chain ancillary ligand was altered.[83] However, in this case the structure of the self-assembled materials was the inverse of that described in this

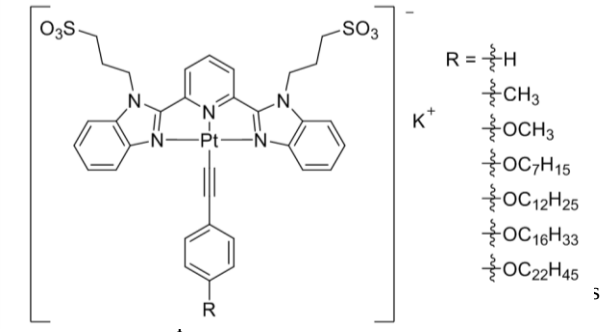

F
s

work as, in the aqueous medium used, the core consisted of hydrophobic pendent alkyl chains and the hydrophilic, charged Pt(II) moieties formed the corona. In this case the transition from fiber to platelet was marked by a corresponding redshift in the emission spectra, suggesting that the inter-complex Pt···Pt spacing varied between morphologies. In contrast, in our work with a core-forming Pt complex, we observed no corresponding redshift in the emission spectra during the morphological transition, indicating that the stacking remains essentially unchanged between fibers and platelets.

Fragmentation of the 2D structures formed by **Pt-PEG$_{12}$** and **Pt-PEG$_7$** was achieved using sonication. We found that the addition of fiber-forming **Pt-PEG$_{16}$** unimer to the fragmented platelets of **Pt-PEG$_{12}$** and **Pt-PEG$_7$** produced scarf-like structures. BCP and homopolymer platelets with crystalline cores have been previously shown to exhibit this behavior as cylinder-forming unimer adds selectively to their open short faces.[84-86]

Rationalizing 2D Structure Formation Through Decreasing PEG Chain Length BCPs with crystallizable core-forming blocks generally form self-assembled structures with a low curvature core-corona interface. By increasing the core-corona block ratio, and therefore decreasing the magnitude of the packing parameter,87,88 a subsequent rise in the inter-coronal repulsion can lead to a more curved interface (*i.e.* the formation of cylinders or fibers compared to platelets).[21] This behavior is also exhibited in the **Pt-PEG$_n$** system, where the steric bulk associated with the oligomer chain length determines the resulting morphology.

The amphiphilic Pt(II) complexes **Pt-PEG$_{12}$** and **Pt-PEG$_7$** initially form 1D structures that slowly, or rapidly, form platelets, respectively. The mechanism for 2D structure formation may involve the fusion of fibers to form 2D platelets. A parallel can be drawn to the self-assembly of PCL-*b*-PEG (PCL = polycaprolactone) BCP/PCL homopolymer blends described by Eisenberg, van de Ven and co-workers in which fibers with a crystalline PCL core form initially and then fuse into "raft" morphologies.[89] By decreasing the bulk of the corona-forming polymeric ligand for the cases of **Pt-PEG$_{16}$** to **Pt-PEG$_{12}$**, we observed a similar morphological transition where 1D fibers form initially and then appear to fuse into large 2D structures with fibers protruding from the platelet ends. Our results suggest that the amphiphilic Pt(II) complexes with shorter solubilizing chains aggregate first into fibers driven by metallophilic and π-stacking interactions and that this is followed by their hierarchical assembly into platelets (see Figures 5d and 8) based on the preference for a lower curvature core-corona interface.

Further characterization of the internal structure of the fibers and platelets revealed several similarities. First, AFM height images of the fibers and platelets formed from **Pt-PEG$_{16}$** and **Pt-PEG$_{12}$** (Figure 4 and 5e respectively) indicated that their height was similar (3.2 nm). This is consistent with the proposed fiber fusion mechanism. Secondly, UV-Vis and fluorescence spectra exhibited no detectable band differences in the region associated with Pt···Pt interactions for the fiber and platelet morphologies (Figure 1). As this absorption band is sensitive with respect to the Pt···Pt stacking distance, this indicates that the packing in the different morphologies is similar. Finally, the assemblies of all three complexes showed a consistent d-spacing of *ca.* 0.32 – 0.33 nm by X-ray and electron diffraction, which is also consistent with the presence of similar stacking of the Pt complexes.

CONCLUSIONS

The seeded-growth living CDSA method developed for BCP self-assembly in 1D and 2D has been successfully extended to stacking square planar Pt(II) complexes that form narrow diameter supramolecular polymeric fibers. Our studies indicate that under conditions where the exchange of the Pt complex building blocks is suppressed, dimensional control is possible. Thus in the cases of the amphiphilic Pt(II) complexes **Pt-PEG$_{16}$** and **Pt-PEG$_{12}$** fibers up to *ca*. 400 nm long with relatively narrow length distributions were accessible *via* seeded growth. Moreover, the fiber length was dependent on the unimer-to-seed mass ratio which is analogous to living covalent polymerizations of molecular monomers.

Samples of **Pt-PEG$_{16}$** fibers displayed no increase in length nor dispersity over the course of 1 week when aged in solution and were therefore static on this timescale. In contrast, both the average length and dispersity of **Pt-PEG$_{12}$** fibers exhibited a substantial increase over a similar 1 week time period, indicating that the fibers were dynamic in solution. Indeed, aging the **Pt-PEG$_{12}$** fibers for 4 weeks revealed the formation of a platelet morphology alongside the initial fibers. By further shortening the PEG chain length to **Pt-PEG$_{7}$**, we were able to exclusively form platelets in under 24 h. This demonstrates that access to supramolecular 1D and 2D architectures can be achieved by simple alterations in the length of the solubilizing ancillary ligand and that this follows the expected trend based on packing parameters. The increase in dynamic behavior in the order **Pt-PEG$_{16}$** < **Pt-PEG$_{12}$** < **Pt-PEG$_{7}$** underscores the necessity for the presence of a long solubilizing ligand in order to suppress dynamic exchange.

Further studies of the 1D and 2D assemblies by electronic absorption, electron and atomic force microscopy and X-ray scattering techniques demonstrated structural similarities between the morphologies. Both exhibited the same UV-vis absorption (centered at 430 nm) and emission (centered at 560 nm where λ_{ex} = 430 nm) behavior which suggested the presence of similar Pt···Pt interactions. Similarly, X-ray scattering and electron diffraction displayed a consistent d spacing of *ca.* 0.32 – 0.33 nm in all 3 self-assembled amphiphilic Pt(II) complexes which we assign to the cofacial stacking repeat distance. AFM also revealed identical heights for the fibers and platelets within experimental error (3.2 nm). It therefore appears likely that when the fibers formed initially by **Pt-PEG$_{12}$** and **Pt-PEG$_{7}$** begin to aggregate they laterally fuse, to form platelets (Figure 5d), a mechanism recently proposed for PCL-based BCP/homopolymer blends.[89]

Both **Pt-PEG$_{12}$** and **Pt-PEG$_{7}$** platelets were fragmented by sonication into smaller surface area and aspect ratio seed structures. By mixing these small square-edged platelets with fiber-growing unimer (*e.g.* **Pt-PEG$_{16}$**), we were able to access hierarchical "scarf-like" architectures. Kinetically-controlled, seeded growth methods analogous to those we describe here should be applicable to a wide range of different supramolecular fiber-forming molecular building blocks. Studies are underway to investigate this possibility, which would allow access a wide range of uniform, functional, and hierarchical[90] materials with diverse potential applications.

METHODS

Synthesis of Pyridyl-PEG$_n$. All reactions were carried out under atmospheres of dry nitrogen using standard Schlenk line techniques. All chemicals were purchased from Aldrich and were used as received unless otherwise stated. The experimental procedure performed for all three derivatives were carried out in a similar fashion. A detailed outline of this procedure for **Pyridyl-PEG$_{16}$** is as follows: **Ts-PEG$_{16}$** (1.5 g, 1.6 mmol, 1.0 eq.), K_2CO_3 (0.24 g, 1.8 mmol, 1.1 eq.) and 4-hydroxypyridine (0.16 g, 1.6 mmol, 1.0 eq.) were dissolved in MeCN (100 mL) and refluxed for 16 h. MeCN was removed under vacuum and a mixture of water (50 mL) and DCM (50 mL) was added. The product was extracted into dichloromethane, washed with brine (1 × 50mL), dried over $MgSO_4$, filtered, and concentrated under reduced pressure. The crude product was then purified by silica gel chromatography using a 10% methanol in DCM mixture to give a light brown oil.

Synthesis of Pt-PEG$_n$. The experimental procedure performed for all three derivatives were carried out in a similar fashion. A detailed outline of this procedure for **Pt-PEG$_{16}$** is as follows: In an argon atmosphere MBraun MB150B-G glove box, **Pyridyl-PEG$_{16}$** (0.16 g, 0.20 mmol, 1.0 eq.), 2,6-bis(tetrazol-5-yl)pyridine[91] (42 mg, 0.20 mmol, 1.0 eq.), $Pt(DMSO)_2Cl_2$ (88 mg, 0.20 mmol, 1.0 eq.) and *N*,*N*-diisopropylethylamine (DIPEA) (78 mg, 0.60, 3.0 eq.) were mixed in MeCN. The reaction mixture was sealed, removed from the glove box and sonicated for 15 min to dissolve all the contained solids. After transferring the reaction mixture to a Schlenk line, it was then refluxed for 24 h. MeCN was removed under vacuum and the crude product was purified by silica chromatography using 10% methanol in DCM as eluent to give final product as a yellow gum.

Characterization. NMR spectra were recorded at ambient temperatures on a Varian 400 spectrometer with all resonances referenced to residual NMR solvent resonances (^{1}H and ^{13}C). MALDI-TOF mass spectrometry experiments of **Pt-PEG$_{16}$**, **Pt-PEG$_{12}$** and **Pt-PEG$_{7}$** were performed using a Bruker Ultraflextreme running in linear mode. Samples were prepared by mixing a solution containing *trans*-2-[3-(4-tert-butylphenyl)-2-methyl-2propenylidene]malonitrile matrix (20 mg/mL in tetrahydrofuran) and a solution of **Pt-PEG$_n$** (1 mg/mL in tetrahydrofuran) in a 1:9 (v/v) ratio. Approximately 1 μL of the mixed solution was deposited onto a stainless steel sample plate and allowed to dry in air. The resulting mass spectra contain a second distribution 28 mass units shifted from the parent distribution that is the result of a fragmentation of the tetrazole rings that leads to the expulsion of N_2.[92,93]

Electronic Absorption Spectroscopy and Spectrofluorometry. UV-vis absorption spectra were obtained on a Lambda 35 spectrometer employing standard quartz cells (1 cm) from 200 to 800 nm. The absorption plots obtained for **Pt-PEG$_n$** were arbitrarily normalized to ensure no overlap of the absorption band at 430 nm. For varying temperature experiments, a magnetic stirrer for single cells holders was used alongside a peltier temperature controller accessory.

Excitation and emission spectra were obtained on a Jasco FP6500 Spectrofluorometer using standard 1 cm path length quartz cuvettes. Solutions were degassed by bubbling N_2 through the solution before spectrum collection. Emission spectra were collected with a λ_{ex} = 430 nm and excitation spectra were collected with a λ_{em} = 560 nm.

Sonication. Micelles were sonicated at 0 °C in a Bandelin Sonorex Digitec sonication bath for specified times (*i.e.* 0.5 h – 3 h).

AFM. Atomic force microscopy images were obtained in ambient conditions utilizing a Multimode VIII with a Nanoscope V controller with PeakForce feedback control. Platelets drop-cast on carbon-coated copper grids were used for AFM measurements. All AFM images from which dimensions were determined were obtained with a fresh SCANASYST-HR (Bruker) cantilever of nominal tip radius 2 nm. The dimensions quoted in the text have not been corrected for tip effects, which are expected to be negligible. Images were analyzed using Gwyddion, an open-source software program for SPM images (www.gwyddion.net).

CLSM. Confocal imaging was performed using a Leica SP5 system attached to a Leica DMI6000 inverted epifluorescence microscope with a ×63 (numerical aperture 1.4) oil immersion objective lens. **Pt-PEG$_n$** was excited using an Argon laser operating at 405 nm. Confocal images were obtained using digital detectors with observation windows of 500-640 nm. The resulting outputs were obtained as digital false-color images, and were color coded as green. Micelle concentrations of 0.05 mg/mL in chloroform were used for imaging experiments.

SAXS and WAXS. X-ray scattering measurements were performed in transmission geometry using a Ganesha small angle X-ray scattering apparatus (SAXSLAB, Denmark). Solution samples were prepared by dissolving the solid Pt complex in DMF (~5 mg/mL), aging for 16 h or 4 weeks at 21 °C, and then sealing a 50 µL aliquot in a capillary tube with Araldite®. To produce a film of for WAXS analysis, the same 5 mg/mL DMF solution was drop-cast onto a 25 µm thick Kapton® film (4,4'-oxydiphenylene-pyromellitimide, DuPont). The capillary or film was then secured in position, perpendicular to the X-ray beam and the detector was positioned at a distance of *ca.* 1050 mm and 100 mm for the SAXS and WAXS measurements respectively. All measurements were carried out in an evacuated chamber to reduce scattering by air. As the instrument has been calibrated to give absolute intensities for each configuration, the data sets could be separately background subtracted and azimuthaly regrouped and subsequently overlaid and stitched together without introducing further scaling factors

TEM and SAED: The samples for electron microscopy were prepared by drop-casting one drop (*ca*. 10 µL) of the colloidal solution onto a carbon coated copper grid which was placed on a piece of filter paper to remove excess solvent. Bright field TEM micrographs were obtained on a JEOL1200EX II microscope equipped with an SIS MegaViewIII digital camera or JEOL1400 microscope equipped with a Gatan Orius 830 digital camera. Both microscopes were operated at 120 kV. No staining of the samples was necessary. Images were analyzed using the ImageJ software package developed at the US National Institute of Health. For the statistical length analysis, 180 - 230 cylinders were carefully traced by hand to determine the contour length or surface area. From this data L_n and L_w of each sample of fibers were calculated as shown below (L = length of object, N = number).

$$L_n = \frac{\sum_{i=1}^{n} N_i L_i}{\sum_{i=1}^{n} N_i} \qquad L_w = \frac{\sum_{i=1}^{n} N_i L_i^2}{\sum_{i=1}^{n} N_i L_i}$$

The standard deviations (σ) of the measured lengths are related to length dispersity (L_w/L_n) assuming a Gaussian distribution through the following expression:[94,95]

$$\frac{L_w}{L_n} - 1 = (\frac{\sigma}{L_n})^2$$

Gaussian distribution functions overlaying relevant histograms were plotted according to the probability density function of a normal distribution as shown in the following equation:

$$f(x|L_n, \sigma) = \frac{1}{\sigma\sqrt{2\pi}} e^{-\frac{(x-L_n)^2}{2\sigma^2}}$$

Where L_n is the mean contour length of the measured fibers and σ is the standard deviation.

Electron diffraction (ED) patterns for the fibers and platelets were collected by Philips CM200 LaB6 TEM equipped with a 4 pi imaging system with a spotsize of 10 at 200kV. The d-spacing values for the SAED patterns were calibrated using AuNP standards.

ASSOCIATED CONTENT

The relevant supporting information regarding **Pt-PEG$_n$** complex synthesis and self-assembly can be found free of charge on the ACS Publications website at DOI: 10.1021/acsnano.XXXXX. Detailed self-assembly conditions and nanostructure size data (in histogram form) with accompanying TEM and/or AFM images for all homogeneous nucleation, sonication and seeded-growth experiments are included. WAXS, SAXS and SAED plots are also contained within and labeled in sections corresponding to their appearance in this manuscript.

AUTHOR INFORMATION

Corresponding Author

ian.manners@bristol.ac.uk

ACKNOWLEDGMENT

M.E.R is grateful to the University of Bristol and EPSRC for funding. A.N. is grateful to the European Union for a Marie Curie Fellowship. D.W.H was supported by the EPSRC Doctoral Training Centre grant [EP/G036780]. D.J.L and C.E.B thank the Bristol Chemical Synthesis Centre for Doctoral Training, funded by EPSRC, for a PhD studentship [EP/G036764/1]. TEM and PeakForce AFM was carried out in the Chemical Imaging Facility, University of Bristol with equipment funded by the University of Bristol and the EPSRC (EP/K035746/1 and EP/M028216/1) under the "*Atoms to Applications*" grant.

REFERENCES

(1) De Greef, T. F. A.; Smulders, M. M. J.; Wolffs, M.; Schenning, A. P. H. J.; Sijbesma, R. P.; Meijer, E. W. Supramolecular Polymerization. *Chem. Rev.*, **2009**, *109*, 5687-5754.

(2) Sijbesma, R. P.; Beijer, F. H.; Brunsveld, L.; Folmer, B. J. B.; Hirschberg, J.; Lange, R. F. M.; Lowe, J. K. L.; Meijer, E. W. Reversible Polymers Formed from Self-Complementary Monomers Using Quadruple Hydrogen Bonding. *Science*, **1997**, *278*, 1601-1604.

(3) Aida, T.; Meijer, E. W.; Stupp, S. I. Functional Supramolecular Polymers. *Science*, **2012**, *335*, 813-817.

(4) Rest, C.; Kandanelli, R.; Fernandez, G. Strategies to Create Hierarchical Self-Assembled Structures *via* Cooperative Non-Covalent Interactions. *Chem. Soc. Rev.*, **2015**, *44*, 2543-2572.

(5) Yang, L.; Tan, X.; Wang, Z.; Zhang, X. Supramolecular Polymers: Historical Development, Preparation,

Characterization, and Functions. *Chem. Rev.*, **2015**, *115*, 7196-7239.
(6) Babu, S. S.; Praveen, V. K.; Ajayaghosh, A. Functional π-Gelators and Their Applications. *Chem. Rev.*, **2014**, *114*, 1973-2129.
(7) Watson, M. D.; Fechtenkötter, A.; Müllen, K. Big Is Beautiful−"Aromaticity" Revisited from the Viewpoint of Macromolecular and Supramolecular Benzene Chemistry. *Chem. Rev.*, **2001**, *101*, 1267-1300.
(8) Rowan, S. J. Polymer Self-Assembly: Micelles Make a Living. *Nat. Mater.*, **2009**, *8*, 89-91.
(9) Bosman, A. W.; Sijbesma, R. P.; Meijer, E. W. Supramolecular Polymers at Work. *Materials Today*, **2004**, *7*, 34-39.
(10) Albertazzi, L.; van der Zwaag, D.; Leenders, C. M. A.; Fitzner, R.; van der Hofstad, R. W.; Meijer, E. W. Probing Exchange Pathways in One-Dimensional Aggregates with Super-Resolution Microscopy. *Science*, **2014**, *344*, 491-495.
(11) Kang, J.; Miyajima, D.; Mori, T.; Inoue, Y.; Itoh, Y.; Aida, T. A Rational Strategy for the Realization of Chain-Growth Supramolecular Polymerization. *Science*, **2015**, *347*, 646-651.
(12) Mukhopadhyay, R. D.; Ajayaghosh, A. Living Supramolecular Polymerization. *Science*, **2015**, *349*, 241-242.
(13) Lunn, D. J.; Finnegan, J. R.; Manners, I. Self-Assembly of "Patchy" Nanoparticles: A Versatile Approach to Functional Hierarchical Materials. *Chem. Sci.*, **2015**, *6*, 3663-3673.
(14) van der Zwaag, D.; de Greef, T. F. A.; Meijer, E. W. Programmable Supramolecular Polymerizations. *Angew. Chem. Int. Ed.*, **2015**, *54*, 8334-8336.
(15) Huang, Z.; Yang, L.; Liu, Y.; Wang, Z.; Scherman, O. A.; Zhang, X. Supramolecular Polymerization Promoted and Controlled through Self-Sorting. *Angew. Chem. Int. Ed.*, **2014**, *53*, 5351-5355.
(16) Zhang, Q.; Tian, H. Effective Integrative Supramolecular Polymerization. *Angew. Chem. Int. Ed.*, **2014**, *53*, 10582-10584.
(17) Kumar, J.; Tsumatori, H.; Yuasa, J.; Kawai, T.; Nakashima, T. Self-Discriminating Termination of Chiral Supramolecular Polymerization: Tuning the Length of Nanofibers. *Angew. Chem. Int. Ed.*, **2015**, *54*, 5943-5947.
(18) Odian, G., in *Principles of Polymerization*, Eds, John Wiley & Sons, Inc., New Jersey, 2004.
(19) Mullin, J. W., *Crystallization*, Oxford: Butterworth-Heinemann, 1993.
(20) Massey, J. A.; Temple, K.; Cao, L.; Rharbi, Y.; Raez, J.; Winnik, M. A.; Manners, I. Self-assembly of Organometallic Block Copolymers: The Role of Crystallinity of the Core-Forming Polyferrocene Block in the Micellar Morphologies Formed by Poly(ferrocenylsilane-b-dimethylsiloxane) in N-Alkane Solvents. *J. Am. Chem. Soc.*, **2000**, *122*, 11577-11584.
(21) Cao, L.; Manners, I.; Winnik, M. A. Influence of the Interplay of Crystallization and Chain Stretching on Micellar Morphologies: Solution Self-Assembly of Coil−Crystalline Poly(isoprene-block-ferrocenylsilane). *Macromolecules*, **2002**, *35*, 8258-8260.
(22) Du, Z.-X.; Xu, J.-T.; Fan, Z.-Q. Micellar Morphologies of Poly(ε-caprolactone)-b-poly(ethylene oxide) Block Copolymers in Water with a Crystalline Core. *Macromolecules*, **2007**, *40*, 7633-7637.
(23) Fujiwara, T.; Miyamoto, M.; Kimura, Y.; Iwata, T.; Doi, Y. Self-Organization of Diblock and Triblock Copolymers of Poly(l-lactide) and Poly(oxyethylene) into Nanostructured Bands and Their Network System. Proposition of a Doubly Twisted Chain Conformation of Poly(l-lactide). *Macromolecules*, **2001**, *34*, 4043-4050.
(24) Zhang, J.; Wang, L.-Q.; Wang, H.; Tu, K. Micellization Phenomena of Amphiphilic Block Copolymers Based on Methoxy Poly(ethylene glycol) and Either Crystalline or Amorphous Poly(caprolactone-b-lactide). *Biomacromolecules*, **2006**, *7*, 2492-2500.
(25) Schmalz, H.; Schmelz, J.; Drechsler, M.; Yuan, J.; Walther, A.; Schweimer, K.; Mihut, A. M. Thermo-Reversible Formation of Wormlike Micelles with a Microphase-Separated Corona from a Semicrystalline Triblock Terpolymer. *Macromolecules*, **2008**, *41*, 3235-3242.
(26) Lee, E.; Hammer, B.; Kim, J.-K.; Page, Z.; Emrick, T.; Hayward, R. C. Hierarchical Helical Assembly of Conjugated Poly(3-hexylthiophene)-block-poly(3-triethylene glycol thiophene) Diblock Copolymers. *J. Am. Chem. Soc.*, **2011**, *133*, 10390-10393.
(27) Lazzari, M.; Scalarone, D.; Hoppe, C. E.; Vazquez-Vazquez, C.; Lòpez-Quintela, M. A. Tunable Polyacrylonitrile-Based Micellar Aggregates as a Potential Tool for the Fabrication of Carbon Nanofibers. *Chem. Mater.*, **2007**, *19*, 5818-5820.
(28) Sun, L.; Pitto-Barry, A.; Kirby, N.; Schiller, T. L.; Sanchez, A. M.; Dyson, M. A.; Sloan, J.; Wilson, N. R.; O'Reilly, R. K.; Dove, A. P. Structural Reorganization of Cylindrical Nanoparticles Triggered by Polylactide Stereocomplexation. *Nat. Commun.*, **2014**, *5*, 5746.
(29) Zhao, D.; Moore, J. S. Nucleation-Elongation: a Mechanism for Cooperative Supramolecular Polymerization. *Org. Biomol. Chem.*, **2003**, *1*, 3471-3491.
(30) Wang, X.; Guerin, G.; Wang, H.; Wang, Y.; Manners, I.; Winnik, M. A. Cylindrical Block Copolymer Micelles and Co-Micelles of Controlled Length and Architecture. *Science*, **2007**, *317*, 644-647.
(31) Gilroy, J. B.; Gädt, T.; Whittell, G. R.; Chabanne, L.; Mitchels, J. M.; Richardson, R. M.; Winnik, M. A.; Manners, I. Monodisperse Cylindrical Micelles by Crystallization-Driven Living Self-Assembly. *Nat. Chem.*, **2010**, *2*, 566-570.
(32) Guérin, G.; Wang, H.; Manners, I.; Winnik, M. A. Fragmentation of Fiberlike Structures: Sonication Studies of Cylindrical Block Copolymer Micelles and Behavioral Comparisons to Biological Fibrils. *J. Am. Chem. Soc.*, **2008**, *130*, 14763-14771.
(33) Boott, C. E.; Gwyther, J.; Harniman, R. L.; Hayward, D. W.; Manners, I. Scalable and Uniform 1D Nanoparticles by Synchronous Polymerization, Crystallization and Self-Assembly. *Nat. Chem.*, **2017**, *9*, 785-792.
(34) Wang, H.; Lin, W.; Fritz, K. P.; Scholes, G. D.; Winnik, M. A.; Manners, I. Cylindrical Block Co-Micelles with Spatially Selective Functionalization by Nanoparticles. *J. Am. Chem. Soc.*, **2007**, *129*, 12924-12925.
(35) Rupar, P. A.; Chabanne, L.; Winnik, M. A.; Manners, I. Non-Centrosymmetric Cylindrical Micelles by Unidirectional Growth. *Science*, **2012**, *337*, 559-562.
(36) Qiu, H.; Gao, Y.; Boott, C. E.; Gould, O. E. C.; Harniman, R. L.; Miles, M. J.; Webb, S. E. D.; Winnik, M. A.; Manners, I. Uniform Patchy and Hollow Rectangular Platelet Micelles from Crystallizable Polymer Blends. *Science*, **2016**, *352*, 697-701.
(37) Li, X.; Gao, Y.; Harniman, R.; Winnik, M.; Manners, I. Hierarchical Assembly of Cylindrical Block Comicelles Mediated by Spatially Confined Hydrogen-Bonding Interactions. *J. Am. Chem. Soc.*, **2016**, *138*, 12902-12912.

(38) Yam, V. W.-W.; Au, V. K.-M.; Leung, S. Y.-L. Light-Emitting Self-Assembled Materials Based on d8 and d10 Transition Metal Complexes. *Chem. Rev.*, **2015**, *115*, 7589-7728.
(39) Mauro, M.; Aliprandi, A.; Septiadi, D.; Kehr, N. S.; De Cola, L. When Self-Assembly Meets Biology: Luminescent Platinum Complexes for Imaging Applications. *Chem. Soc. Rev.*, **2014**, *43*, 4144-4166.
(40) Fu, T.-F.; Ao, L.; Gao, Z.-C.; Zhang, X.-L.; Wang, F. Advances on Supramolecular Assembly of Cyclometalated Platinum(II) Complexes. *Chin. Chem. Lett.*, **2016**, *27*, 1147-1154.
(41) Strassert, C. A.; Mauro, M.; De Cola, L. Photophysics of Soft and Hard Molecular Assemblies Based on Luminescent Complexes. *Adv. Inorg. Chem.*, **2011**, *63*, 47-103.
(42) Tsai, J. L.-L.; Zou, T.; Liu, J.; Chen, T.; Chan, A. O.-Y.; Yang, C.; Lok, C.-N.; Che, C.-M. Luminescent Platinum(II) Complexes with Self-Assembly and Anti-Cancer Properties: Hydrogel, pH Dependent Emission Color and Sustained-Release Properties Under Physiological Conditions. *Chem. Sci.*, **2015**, *6*, 3823.
(43) Yan, X.; Li, S.; Cook, T. R.; Ji, X.; Yao, Y.; Pollock, J. B.; Shi, Y.; Yu, G.; Li, J.; Huang, F.; Stang, P. J. Hierarchical Self-Assembly: Well-Defined Supramolecular Nanostructures and Metallohydrogels *via* Amphiphilic Discrete Organoplatinum(II) Metallacycles. *J. Am. Chem. Soc.*, **2013**, *135*, 14036-14039.
(44) Chen, M.; Wei, C.; Tao, J.; Wu, X.; Huang, N.; Zhang, G.; Li, L. Supramolecular Polymers Self-Assembled from *trans*-Bis(pyridine) Dichloropalladium(II) and Platinum(II) Complexes. *Chem. Eur. J.*, **2014**, *20*, 2812-2818.
(45) Zhang, J.-J.; Lu , W.; Sun, R. W.-Y.; Che, C.-M. Organogold(III) Supramolecular Polymers for Anticancer Treatment. *Angew. Chem. Int. Ed.*, **2012**, *51*, 4882-4886.
(46) Xiao, X.-S.; Kwong, W.-L.; Guan, X.; Yang, C.; Lu, W.; Che, C.-M. Platinum(II) and Gold(III) Allenylidene Complexes: Phosphorescence, Self-Assembled Nanostructures and Cytotoxicity. *Chem. Eur. J.*, **2013**, *19*, 9457-9462.
(47) Au, V. K.-M.; Wu, D.; Yam, V. W.-W. Organic Memory Devices Based on a Bis-Cyclometalated Alkynylgold(III) Complex. *J. Am. Chem. Soc.*, **2015**, *137*, 4654-4657.
(48) Yam, V. W.-W.; Wong, K. M.-C.; Zhu, N. Solvent-Induced Aggregation through Metal···Metal/π···π Interactions: Large Solvatochromism of Luminescent Organoplatinum(II) Terpyridyl Complexes. *J. Am. Chem. Soc.*, **2002**, *124*, 6506-6507.
(49) Komiya, N.; Muraoka, T.; Iida, M.; Miyanaga, M.; Takahashi, K.; Naota, T. Ultrasound-Induced Emission Enhancement Based on Structure-Dependent Homo- and Heterochiral Aggregations of Chiral Binuclear Platinum Complexes. *J. Am. Chem. Soc.*, **2011**, *133*, 16054-16061.
(50) Sambri, L.; Cucinotta, F.; Paoli, G. D.; Stagni, S.; Cola, L. D. Ultrasound-Promoted Hydrogelation of Terpyridine Derivatives. *New J. Chem.*, **2010**, *34*, 2093-2096.
(51) Liu, N.; Wang, B.; Liu, W.; Bu, W. Reversible Luminescence Switching Accompanied by Assembly-Disassembly of Metallosupramolecular Amphiphiles Based on a Platinum(II) Complex. *J. Chem. Mater. Chem. C.*, **2013**, *1*, 1130-1136.
(52) Po, C.; Tam, A. Y.-Y.; Wong, K. M.-C.; Yam, V. W.-W. Supramolecular Self-Assembly of Amphiphilic Anionic Platinum(II) Complexes: A Correlation between Spectroscopic and Morphological Properties. *J. Am. Chem. Soc.*, **2011**, *133*, 12136-12143.
(53) Yuen, M.-Y.; Roy, V. A. L.; Lu, W.; Kui, S. C. F.; Tong, G. S. M.; So, M.-H.; Chui, S. S.-Y.; Muccini, M.; Ning, J. Q.; Xu, S. J.; Che, C.-M. Semiconducting and Electroluminescent Nanowires Self-Assembled from Organoplatinum(II) Complexes. *Angew. Chem. Int. Ed.*, **2008**, *47*, 9895-9899.
(54) Lu, W.; Chui, S. S.-Y.; Ng, K.-M.; Che, C.-M. A Submicrometer Wire-to-Wheel Metamorphism of Hybrid Tridentate Cyclometalated Platinum(II) Complexes. *Angew. Chem. Int. Ed.*, **2008**, *47*, 4568-4572.
(55) Au-Yeung, H.-L.; Tam, A. Y.-Y.; Leung, S. Y.-L.; Yam, V. W.-W. Supramolecular Assembly of Platinum-Containing Polyhedral Oligomeric Silsesquioxanes: an Interplay of Intermolecular Interactions and a Correlation Between Structural Modifications and Morphological Transformations. *Chem. Sci.*, **2017**, *8*, 2267-2276
(56) Aliprandi, A.; Croisetu, C. M.; Mauro, M.; Cola, L. D. Chiral Amplification by Self-Assembly of Neutral Luminescent Platinum(II) Complexes. *Chem. Eur. J.*, **2017**, *23*, 5957-5961.
(57) Xiang, Y.; Li, W.; Fang, Y.; Zhang, D.; Li, X.; Jin, W. Construction and Luminescence Property of a Highly Ordered 2D Self-Assembled Amphiphilic Bidentate Organoplatinum(II) Complex. *RSC Adv.* **2016**, *6*, 27360-27369.
(58) Zhang, X.; Wright, A. M.; DeYonker, N. J.; Hollis, T. K.; Hammer, N. I.; Webster, C. E.; Valente, E. J. Synthesis, Air Stability, Photobleaching, and DFT Modeling of Blue Light Emitting Platinum CCC-N-Heterocyclic Carbene Pincer Complexes. *Organometallics*, **2012**, *31*, 1664-1672.
(59) Zhang, W.; Jin, W.; Fukushima, T.; Saeki, A.; Seki, S.; Aida, T. Supramolecular Linear Heterojunction Composed of Graphite-Like Semiconducting Nanotubular Segments. *Science*, **2011**, *334*, 340-343.
(60) Zhang, W.; Jin, W.; Fukushima, T.; Mori, T.; Aida, T. Helix Sense-Selective Supramolecular Polymerization Seeded by a One-Handed Helical Polymeric Assembly. *J. Am. Chem. Soc.*, **2015**, *137*, 13792-13795.
(61) Ma, X.; Zhang, Y.; Zhang, Y.; Liu, Y.; Che, Y.; Zhao, J. Fabrication of Chiral-Selective Nanotubular Heterojunctions through Living Supramolecular Polymerization. *Angew. Chem. Int. Ed.*, **2016**, *55*, 9539-9543.
(62) Ogi, S.; Fukui, T.; Jue, M. L.; Takeuchi, M.; Sugiyasu, K. Kinetic Control over Pathway Complexity in Supramolecular Polymerization through Modulating the Energy Landscape by Rational Molecular Design. *Angew. Chem. Int. Ed.*, **2014**, *53*, 14363-14367.
(63) Endo, M.; Fukui, T.; Jung, S. H.; Yagai, S.; Takeuchi, M.; Sugiyasu, K. Photoregulated Living Supramolecular Polymerization Established by Combining Energy Landscapes of Photoisomerization and Nucleation–Elongation Processes. *J. Am. Chem. Soc.*, **2016**, *138*, 14347-14353.
(64) Fukui, T.; Kawai, S.; Fujinuma, S.; Matsushita, Y.; asuda, T.; Sakurai, T.; Seki, S.; Takeuchi, M.; Sugiyasu, K. Control Over Differentiation of a Metastable Supramolecular Assembly in One and Two Dimensions. *Nat. Chem.*, **2017**, *9*, 493-499.
(65) Ogi, S.; Stepanenko, V.; Sugiyasu, K.; Takeuchi, M.; Würthner, F. Mechanism of Self-Assembly Process and Seeded Supramolecular Polymerization of Perylene Bisimide Organogelator. *J. Am. Chem. Soc.*, **2015**, *137*, 3300-3307.
(66) Gorl, D.; Zhang, X.; Stepanenko, V.; Wurthner, F. Supramolecular Block Copolymers by Kinetically Controlled Co-Self-Assembly of Planar and Core-Twisted Perylene Bisimides. *Nat. Commun.*, **2015**, *6*, 7009.

(67) Greciano, E. E.; Sánchez, L. Seeded Supramolecular Polymerization in a Three-Domain Self-Assembly of an N-Annulated Perylenetetracarboxamide. *Chem. Eur. J.*, **2016**, *22*, 13724-13730.

(68) Beun, L. H.; Albertazzi, L.; van der Zwaag, D.; de Vries, R.; Cohen Stuart, M. A. Unidirectional Living Growth of Self-Assembled Protein Nanofibrils Revealed by Super-resolution Microscopy. *ACS Nano*, **2016**, *10*, 4973-4980.

(69) Pal, A.; Malakoutikhah, M.; Leonetti, G.; Tezcan, M.; Colomb-Delsuc, M.; Nguyen, V. D.; van der Gucht, J.; Otto, S. Controlling the Structure and Length of Self-Synthesizing Supramolecular Polymers through Nucleated Growth and Disassembly. *Angew. Chem. Int. Ed.*, **2015**, *54*, 7852-7856.

(70) Robinson, M. E.; Lunn, D. J.; Nazemi, A.; Whittell, G. R.; De Cola, L.; Manners, I. Length Control of Supramolecular Polymeric Nanofibers Based on Stacked Planar Platinum(II) Complexes by Seeded-Growth. *Chem. Commun.*, **2015**, *51*, 15921-15924.

(71) For a recent report on the seeded growth of a Pt(II) complex analogous to the species studied here but without long solvophilic ancillarly ligation that gives univorm large diameter fiber-like rods on a much longer (multi-micron) length scale, see: Aliprandi, A.; Mauro, M.; De Cola, L. Controlling and Imaging Biomimetic Self-Assembly. *Nat. Chem.*, **2016**, *8*, 10-15.

(72) Strassert, C. A.; Chien, C.-H.; Galvez Lopez, M. D.; Kourkoulos, D.; Hertel, D.; Meerholz, K.; De Cola, L. Switching On Luminescence by the Self-Assembly of a Platinum(II) Complex into Gelating Nanofibers and Electroluminescent Films. *Angew. Chem. Int. Ed.*, **2011**, *50*, 946-950.

(73) Mauro, M.; Aliprandi, A.; Cebrian, C.; Wang, D.; Kubel, C.; De Cola, L. Self-Assembly of a Neutral Platinum(II) Complex into Highly Emitting Microcrystalline Fibers Through Metallophilic Interactions. *Chem. Commun.*, **2014**, *50*, 7269-7272.

(74) Allampally, N. K.; Strassert, C. A.; De Cola, L. Luminescent Gels by Self-Assembling Platinum complexes. *Dalton Trans.*, **2012**, *41*, 13132-13137.

(75) Mydlak, M.; Mauro, M.; Polo, F.; Felicetti, M.; Leonhardt, J.; Diener, G.; De Cola, L.; Strassert, C. A. Controlling Aggregation in Highly Emissive Pt(II) Complexes Bearing Tridentate Dianionic N^N^N Ligands. Synthesis, Photophysics, and Electroluminescence. *Chem. Mater.*, **2011**, *23*, 3659-3667.

(76) Williams, J. A. G., in *Photochemistry and Photophysics of Coordination Compounds II*, Eds: V. Balzani and S. Campagna, Springer Berlin Heidelberg, 2007.

(77) Yam, V. W.-W.; Chan, K. H.-Y.; Wong, K. M.-C.; Zhu, N. Luminescent Platinum(II) Terpyridyl Complexes: Effect of Counter Ions on Solvent-Induced Aggregation and Color Changes. *Chem. Eur. J.*, **2005**, *11*, 4535-4543.

(78) Shen, L.; Wang, H.; Guerin, G.; Wu, C.; Manners, I.; Winnik, M. A. A Micellar Sphere-to-Cylinder Transition of Poly(ferrocenyldimethylsilane-b-2-vinylpyridine) in a Selective Solvent Driven by Crystallization. *Macromolecules*, **2008**, *41*, 4380-4389.

(79) Tam, A. Y.-Y.; Wong, K. M.-C.; Wang, G.; Yam, V. W.-W. Luminescent Metallogels of Platinum(II) Terpyridyl Complexes: Interplay of Metal···Metal, π-π and Hydrophobic-Hydrophobic Interactions on Gel Formation. *Chem. Commun.*, **2007**, 2028-2030.

(80) Tam, A.-Y.; Wong, K.-C.; Zhu, N.; Wang, G.; Yam, V.-W. Luminescent Alkynylplatinum(II) Terpyridyl Metallogels Stabilized by Pt···Pt, π−π, and Hydrophobic−Hydrophobic Interactions. *Langmuir*, **2009**, *25*, 8685-8695.

(81) Ai, Y.; Li, Y.; Ma, H.; Su, C.-Y.; Yam, V. W.-W. Cyclometalated Platinum(II) Complexes of 1,3-Bis(1-n-butylpyrazol-3-yl)benzenes: Synthesis, Characterization, Electrochemical, Photophysical, and Gelation Behavior Studies. *Inorg. Chem.*, **2016**, *55*, 11920-11929.

(82) Gwyther, J.; Gilroy, J. B.; Rupar, P. A.; Lunn, D. J.; Kynaston, E.; Patra, S. K.; Whittell, G. R.; Winnik, M. A.; Manners, I. Dimensional Control of Block Copolymer Nanofibers with a π-Conjugated Core: Crystallization-Driven Solution Self-Assembly of Amphiphilic Poly(3-hexylthiophene)-b-poly(2-vinylpyridine). *Chem. Eur. J.*, **2013**, *19*, 9186-9197.

(83) Po, C.; Tam, A. Y.-Y.; Yam, V. W.-W. Tuning of Spectroscopic Properties *via* Variation of the Alkyl Chain Length: A Systematic Study of Molecular Structural Changes on Self-Assembly of Amphiphilic Sulfonate-Pendant Platinum(II) Bzimpy Complexes in Aqueous Medium. *Chem. Sci.*, **2014**, *5*, 2688-2695.

(84) Gadt, T.; Ieong, N. S.; Cambridge, G.; Winnik, M. A.; Manners, I. Complex and Hierarchical Micelle Architectures from Diblock Copolymers Using Living, Crystallization-Driven Polymerizations. *Nat. Mater.*, **2009**, *8*, 144-150.

(85) Rupar, P. A.; Cambridge, G.; Winnik, M. A.; Manners, I. Reversible Cross-Linking of Polyisoprene Coronas in Micelles, Block Comicelles, and Hierarchical Micelle Architectures Using Pt(0)–Olefin Coordination. *J. Am. Chem. Soc.*, **2011**, *133*, 16947-16957.

(86) He, X.; Hsiao, M.-S.; Boott, C. E.; Harniman, R. L.; Nazemi, A.; Li, X.; Winnik, M. A.; Manners, I. Two-Dimensional Assemblies from Crystallizable Homopolymers with Charged Termini. *Nat. Mater.*, **2017**, *16*, 481-488.

(87) Nagarajan, R. Molecular Packing Parameter and Surfactant Self-Assembly: The Neglected Role of the Surfactant Tail. *Langmuir*, **2002**, *18*, 31-38.

(88) Israelachvili, J. N.; Mitchell, D. J.; Ninham, B. W. Theory of Self-Assembly of Hydrocarbon Amphiphiles into Micelles and Bilayers. *J. Chem. Soc., Faraday Trans. 2*, **1976**, *72*, 1525-1568.

(89) Rizis, G.; van de Ven, T. G. M.; Eisenberg, A. "Raft" Formation by Two-Dimensional Self-Assembly of Block Copolymer Rod Micelles in Aqueous Solution. *Angew. Chem. Int. Ed.*, **2014**, *53*, 9000-9003.

(90) Qiu, H.; Hudson, Z. M.; Winnik, M. A.; Manners, I. Multidimensional Hierarchical Self-Assembly of Amphiphilic Cylindrical Block Comicelles. *Science*, **2015**, *347*, 1329-1332.

(91) 2,6-bis(tetrazol-5-yl)pyridine was synthesized according to the proceudre described in: McManus, J. M.; Herbst, R. M. Tetrazole Analogs of Pyridinecarboxylic Acids. *J. Org. Chem.*, **1959**, *24*, 1462-1464.

(92) Forkey, D. M.; Carpenter, W. R. Mass Spectrometry of Methyltetrazoles. *Org. Mass. Spectrom.*, **1969**, *2*, 433-445.

(93) Raynaud, J.; Absalon, C.; Gnanou, Y.; Taton, D. N-Heterocyclic Carbene-Induced Zwitterionic Ring-Opening Polymerization of Ethylene Oxide and Direct Synthesis of α,ω-Difunctionalized Poly(ethylene oxide)s and Poly(ethylene oxide)-b-poly(ε-caprolactone) Block Copolymers. *J. Am. Chem. Soc.*, **2009**, *131*, 3201-3209.

(94) Henderson, J. F.; Szwarc, M. The Use of Living Polymers in the Preparation of Polymer Structures of Controlled Architecture. *J. Polym. Sci.: Macromol. Rev.*, **1968**, *3*, 317-401.

(95) Rogošić, M.; Mencer, H. J.; Gomzi, Z. Polydispersity Index and Molecular Weight Distributions of Polymers. *Eur. Polym. J.* **1996**, *32*, 1337-1344.